

On the Close Correspondence between Storm-time ULF Wave Power and the POES VLF Chorus Wave Amplitude Proxy

Stavros Dimitrakoudis¹, Ian R. Mann¹

¹Department of Physics, University of Alberta, Edmonton, Alberta, Canada

Key Points:

- There is a common L-shell and time profile of storm-time ground-based ULF wave power and the POES proxy for VLF wave amplitude
- Global ground-based ULF wave power coherence implies a small number of meridians can be used to estimate radial diffusion coefficients
- ULF wave power and the POES VLF wave proxy discriminate identically between efficient and inefficient radiation belt acceleration events

arXiv:1908.08480v1 [physics.space-ph] 22 Aug 2019

Corresponding author: S. Dimitrakoudis, dimitrak@ualberta.ca

Abstract

Ground-based Pc5 ULF wave power in multiple ground-based meridians is compared to the VLF wave amplitude proxy, derived from POES precipitation, for the 33 storms studied by *Li et al.* [2015]. The results reveal common L-shell and time profiles for the ULF waves and VLF proxy for every single storm, especially at $L \leq 6$, and identical discrimination between efficient and inefficient radiation belt electron acceleration. The observations imply either ULF waves play a role in driving precipitation which is falsely interpreted as VLF wave power in the proxy, ULF waves drive VLF waves (the reverse being energetically unfeasible), or both have a common driver with nearly identical L-shell and time-dependence. Global ground-based ULF wave power coherence implies a small number of meridians can be used to estimate storm-time radial diffusion coefficients. However, the strong correspondence between ULF wave power and VLF wave proxy complicates causative assessments of electron acceleration.

1 Introduction

The Earth's outer radiation belt is populated mostly by electrons, which are at times accelerated to relativistic energies ($> 1\text{MeV}$), and can thus pose a danger to satellites and astronauts [*Baker*, 1998; *Webb and Allen*, 2004; *Daglis et al.*, 2004; *Choi et al.*, 2011; *Sarno-Smith et al.*, 2016]. It is therefore important to determine the complete set of processes by which this acceleration takes place, starting with solar wind drivers and ending with changes to electron dynamics near Earth, for the purpose of forecasting and risk mitigation. Two acceleration mechanisms have emerged as favoured candidates for the dominant role in the process: energy diffusion by chorus waves [*Horne and Thorne*, 1998; *Summers et al.*, 2002; *Horne et al.*, 2005; *Tao et al.*, 2009; *Reeves et al.*, 2013; *Thorne et al.*, 2013; *Li et al.*, 2014; *Tu et al.*, 2014; *Li et al.*, 2016], or inward radial diffusion by ultralow frequency (ULF) waves [*Fälthammar*, 1965; *Schulz and Lanzerotti*, 1974; *Elkington et al.*, 1999; *Hudson et al.*, 1999; *Mathie and Mann*, 2000; *Perry et al.*, 2005; *Fei et al.*, 2006; *Ukhorskiy et al.*, 2009; *Huang et al.*, 2010; *Turner et al.*, 2012; *Mann et al.*, 2016; *Cunningham*, 2016].

Li et al. [2015] (henceforth L15) recently applied an indirect method of calculating chorus wave intensity using a VLF wave proxy defined using POES electron precipitation measurements [*Li et al.*, 2013; *Ni et al.*, 2014] to examine the potential role of VLF waves in radiation belt dynamics. L15 compared this VLF proxy to the response of the outer electron radiation belt for 33 storms, which they separated into 16 efficient acceleration (EA) and 17 inefficient acceleration (IA) events based on the relativistic electron response, and found a correlation between the VLF chorus wave proxy and the efficiency of electron acceleration. Since the L15 analysis was only performed using the VLF chorus wave proxy, the question of how well ULF waves correlate with those same events was left open. It was indirectly revisited by *Li et al.* [2016], where diffusion coefficients from chorus waves, ULF radial diffusion, and plasmaspheric hiss were calculated for the 17 March 2015 geomagnetic storm; but the radial diffusion coefficients were derived from analytical expressions [*Brautigam and Albert*, 2000; *Ozeke et al.*, 2014], which are statistically derived, and may not always perfectly correspond to those in each particular event [*Murphy et al.*, 2016]. Here we revisit the events considered by L15 using a new method of visualizing ULF wave power across multiple L-shells, and in multiple MLT meridians, as a function of time by using data from multiple ground magnetometer chains deployed across the Earth's northern hemisphere. The large amount of ULF wave data available from these arrays allows us to perform a ULF wave superposition analysis much like L15 did for chorus waves, and to hence directly compare both the distributions of the ULF wave power and the VLF chorus wave proxy, and their potential role in radiation belt electron acceleration.

We present our methodology in Section 2, our results in Section 3, and conclude with a discussion in Section 4.

2 Methodology

We use the same 16 efficient acceleration (EA) and 17 inefficient acceleration (IA) electron radiation belt events identified by L15 during the period from October 2012 to March 2015. We calculated the integrated Pc5 ULF power every hour for seven days spanning the minimum in electron flux for each one of those storm events. We then superposed the ULF wave data for the EA and IA events separately, in order to produce figures that can be directly comparable to both the VLF chorus wave proxy for each event, and the superposed epoch analysis of the VLF proxy for the EA and IA events, presented in L15. The same VLF chorus wave amplitude proxy derived by L15 is used in this study, where the ratio of POES-observed 30-100 keV electron loss-cone to trapped fluxes averaged over all MLT regions is used to generate a global proxy for VLF wave chorus amplitudes. For direct comparison, in the ULF wave power figures presented below we also show the relevant VLF chorus wave proxy data from L15 in the last panel.

For all events the zero epoch was defined in the same way as L15, being the time when the maximum electron phase space density (PSDmax), taken over the range of $2.5 - 6R_E$ and at first adiabatic invariant ($\mu = 3433\text{MeV/G}$) and second adiabatic invariant ($K = 0.10G^{1/2}R_E$) as measured by the Van Allen Probes Relativistic Electron Proton Telescope (REPT) instrument [Baker *et al.*, 2013; Spence *et al.*, 2013] reaches a minimum. Note also that L15 defined an EA (IA) event if within two days prior to the zero epoch time PSDmax decreased at least by a factor of 5, while within two days after that it was larger (smaller) than $10^{-8}(10^{-9})c^3\text{MeV}^{-3}\text{cm}^{-3}$. This is also the categorization used here.

To build a comprehensive picture of the global nature of ULF wave power as a function of L, MLT and time for these 33 events, we used measurements from 21 selected ground magnetometer stations available from the SuperMAG archive, which offers easy access to standardized data from over 300 ground magnetometers from multiple arrays from around the world [Gjerloev, 2009, 2012]. More specifically, we focused on data from five latitudinal chains of northern stations from different longitude sectors, labelled as Atlantic, Alberta (Canada), Alaska, Siberia, and Scandinavia, at latitudes that correspond to invariant dipole L-shells from $L \sim 2.5$ to $L \sim 6.5$ (cf. Figure 1). For most of the selected stations, data was available for all of the 33 events. However, a small number of the selected stations in key L-shell and longitudinal sectors had some data gaps and in such cases alternative nearby stations were used where possible to try to fill in the coverage. Data from the selected stations are all shown in Figure 1 and their names and coordinates are displayed in Table 1. The SuperMAG data used here was standardized to a 1-minute cadence, so by performing Fast Fourier Transform (FFT) as described in Rae *et al.* [2012] we were able to obtain power spectra in the Pc5 frequency range, from 1.68 to 7mHz, spaced with a uniform linear step of 0.28 mHz. These Pc5 power spectra were derived for each hour, from all of the available selected stations, and their summed power from 1.68 to 7mHz were then plotted in bins of width of one dipole L-shell.

3 Results

Panels a-f in Figure 2 show ULF power for a representative EA event on 8-9 October 2012, which can be compared directly to Figure 1 in L15. We see an extremely strong similarity of the ULF wave power distributions with the L15 POES VLF chorus wave proxy, replotted here in panel f. Both L-shell and time profiles of the ULF wave power with that of the POES VLF chorus are seen to enhance in the day before

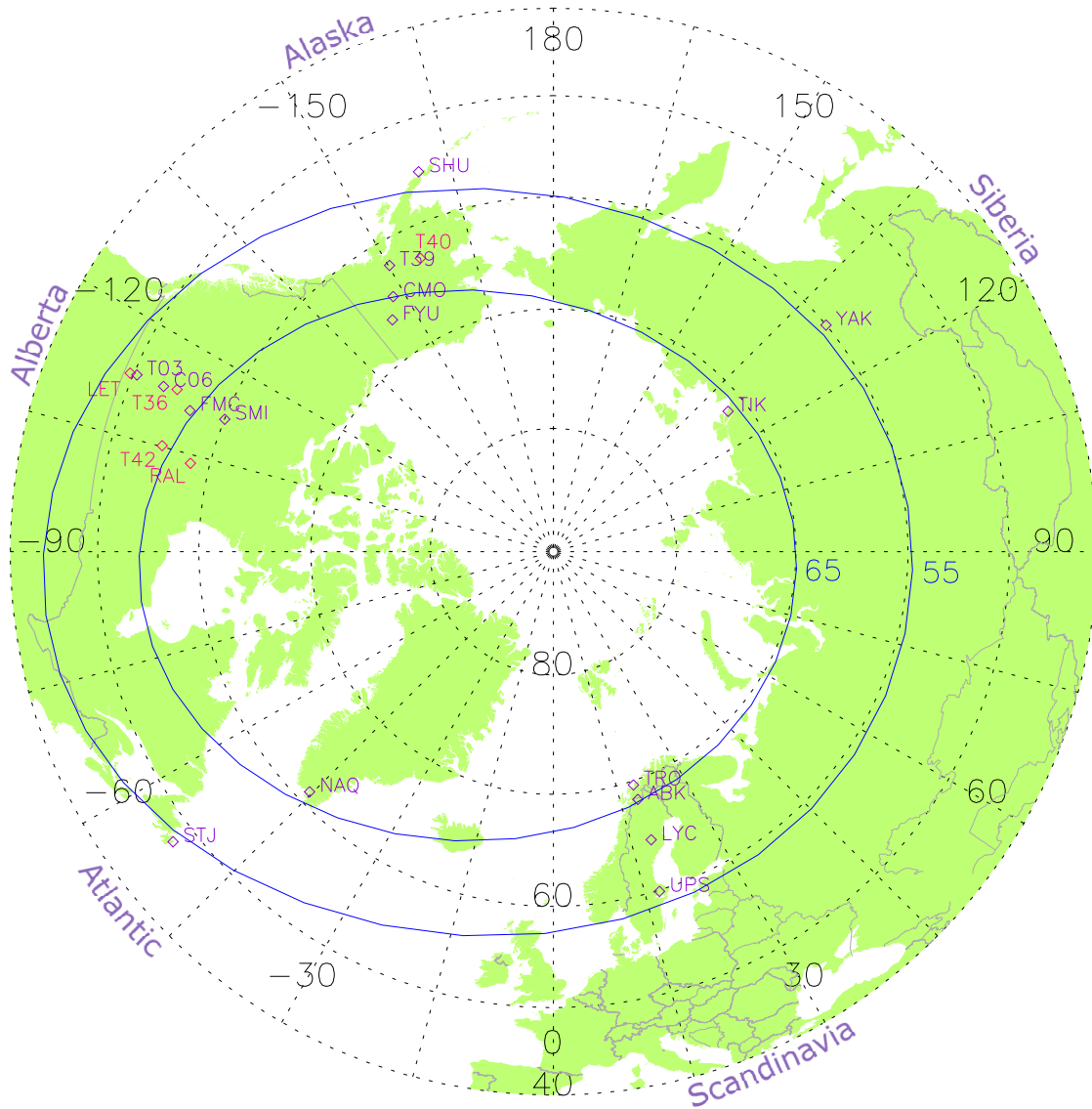


Figure 1. Map of the selected ground magnetometer stations used in this study (cf. Table 1). The stations belonging to the standard set are in purple, while additional temporary replacement stations are shown in magenta. The blue curves are magnetic latitude contours, at 55°N and 65°N in 2013.

Table 1. Ground magnetometer stations used in this work.

Code	Name	Geo. Lat. / Lon. (°)N / (°)E	CGM Lat. / Lon. (°)N / (°)E	L-shell	primary operator
Alaska					
FYU	Fort Yukon	66.56 / 214.79	67.65 / 267.17	6.85	GIMA
CMO	College	64.87 / 212.14	65.45 / 266.18	5.77	GIMA
T39	Trapper Creek	62.30 / 209.80	62.37 / 265.76	4.65	GIMA
SHU	Shumagin	55.38 / 199.54	53.29 / 260.26	2.83	USGS
Alberta					
SMI	Fort Smith	60.03 / 248.07	67.47 / 307.71	6.74	CARISMA
FMC	Fort McMurray	56.66 / 248.79	64.28 / 309.98	5.3	CARISMA
C06	Ministik Lake	53.35 / 247.03	60.64 / 308.76	4.19	CARISMA
T03	Vulcan	50.37 / 247.02	57.60 / 309.60	3.53	CARISMA
Atlantic					
NAQ	Narssarssuaq	61.16 / 314.56	65.75 / 43.19	5.8	DTUSpace
STJ	St Johns	47.60 / 307.32	52.60 / 31.64	2.72	CANMOS
Scandinavia					
TRO	Tromso	69.66 / 18.94	67.07 / 102.77	6.56	IMAGE
ABK	Abisko	68.35 / 18.82	65.74 / 101.70	5.9	IMAGE
LYC	Lycksele	64.61 / 18.75	61.87 / 99.33	4.49	IMAGE
UPS	Uppsala	59.90 / 17.35	56.88 / 95.95	3.35	IMAGE
Siberia					
TIK	Tixie	71.59 / 128.78	66.70 / 198.71	6.4	AARI
YAK	Yakutsk	60.02 / 129.72	54.88 / 202.60	3.05	SHICRA SB RAS & GFZ
Additional stations					
T40	McGrath	63.00 / 204.40	62.16 / 260.84	4.59	THEMIS
RAL	Rabbit Lake	58.22 / 256.32	67.00 / 319.92	6.46	CARISMA
T42	La Ronge	55.15 / 254.84	63.76 / 318.65	5.1	AUTUMN
T36	Athabasca	54.71 / 246.69	61.95 / 307.91	4.54	AUTUMN
LET	Lethbridge	49.64 / 247.13	56.88 / 309.93	3.39	AUTUMN

the minimum flux at epoch time, with each gradually penetrating to lower L-shells during the time that radiation belt flux is decreasing up to epoch time zero (cf. Figure 1 of L15). The subsequent times after epoch time zero, during which the efficient radiation belt acceleration takes place, are accompanied by ongoing enhancements in both ULF wave power and in the POES proxy for VLF chorus wave amplitudes which last for days. What is also immediately apparent is the clear global temporal coherence of the enhancements in ULF wave power spanning all longitudinal meridians, and the extremely close correspondence of these globally coherent ULF wave power enhancements (panels a-e) and those of the global VLF chorus wave amplitude proxy from L15 (panel f).

For comparison, panels g-l show the ULF wave power distributions and the VLF chorus wave amplitude proxy for a characteristic IA event on 1 October 2012 and which can be compared directly to Figure 2 in L15. Once again, there is an obvious and striking similarity between the L-shell and time profiles of the ULF wave power in every longitudinal meridian and the VLF chorus wave amplitude proxy. The characteristic ULF and VLF proxy profiles before epoch time zero for this IA event also look very similar to those for the EA event shown in panels a-f. However, and in contrast to the ULF and VLF characteristics for the EA event in panels a-f, for the IA event in Figure 3 the post epoch time zero ULF and VLF wave power both essentially totally disappear. The only significant difference between the L-shell and time profiles of the ULF wave power and the chorus proxy in all of the panels is the relative lack of activity in the chorus wave proxy at $L > 6$, compared to ULF power which continues to be enhanced at these higher L-shells at the same time. Most likely this can be explained by the relative lack of the equatorial radiation belt electron source population required for electrons to be precipitated and to generate a signal in the POES VLF chorus wave proxy, or alternatively a population of higher L-shell ULF waves which are not associated with POES precipitation. We have completed the same analysis for every one of the remaining 31 storms in the L15 set, and these plots are provided in the Supplementary Material. The extremely close correspondence between the L-shell and time envelopes of the ULF wave power and the POES VLF chorus wave amplitude proxy is maintained in essentially every single event, while a global temporal coherence of the ULF wave power in multiple longitudes is also seen in most events.

Following L15, we also completed a superposed epoch analysis for all of the events in the EA and IA categories, centered around their respective zero epochs. Figure 3, panels (a-e), shows the results from this superposition of ULF wave power in each meridian for the EA events, and this should be compared to the superposed epoch analysis of the VLF wave proxy shown in Figure 3 (f) (reproduced from Figure 3h of L15). Figure 3, panels (g-k) shows the results of the same analysis for the IA events, and where the superposition of the POES VLF chorus amplitude proxy from Figure 3 (l) is the same as that shown in Figure 4h of L15. The characteristics of the superposed ULF wave power from every longitudinal meridian is almost identical to that of the VLF chorus wave proxy in shape in L-shell and time, both for the EA and IA events. Especially for the EA events (Figure 3, panels (a-e)) there appears to be little difference in the ULF wave power profiles between the meridians in different longitudes, and every meridian has the same characteristics as the VLF wave proxy. The same is true for the IA events (Figure 3, panels (g-k)), with perhaps a slightly larger ULF power being seen in the Scandinavian meridian as compared to the other meridians. Overall, just as in the case of the individual EA and IA events (Figure 2), the superposed epoch ULF wave profiles are almost identical to those of the VLF chorus wave amplitude proxy. Figure 4 shows probability distribution plots for all EA and IA events, demonstrating that high values of integrated ULF power predominantly coincide with high amplitudes of the VLF chorus wave proxy.

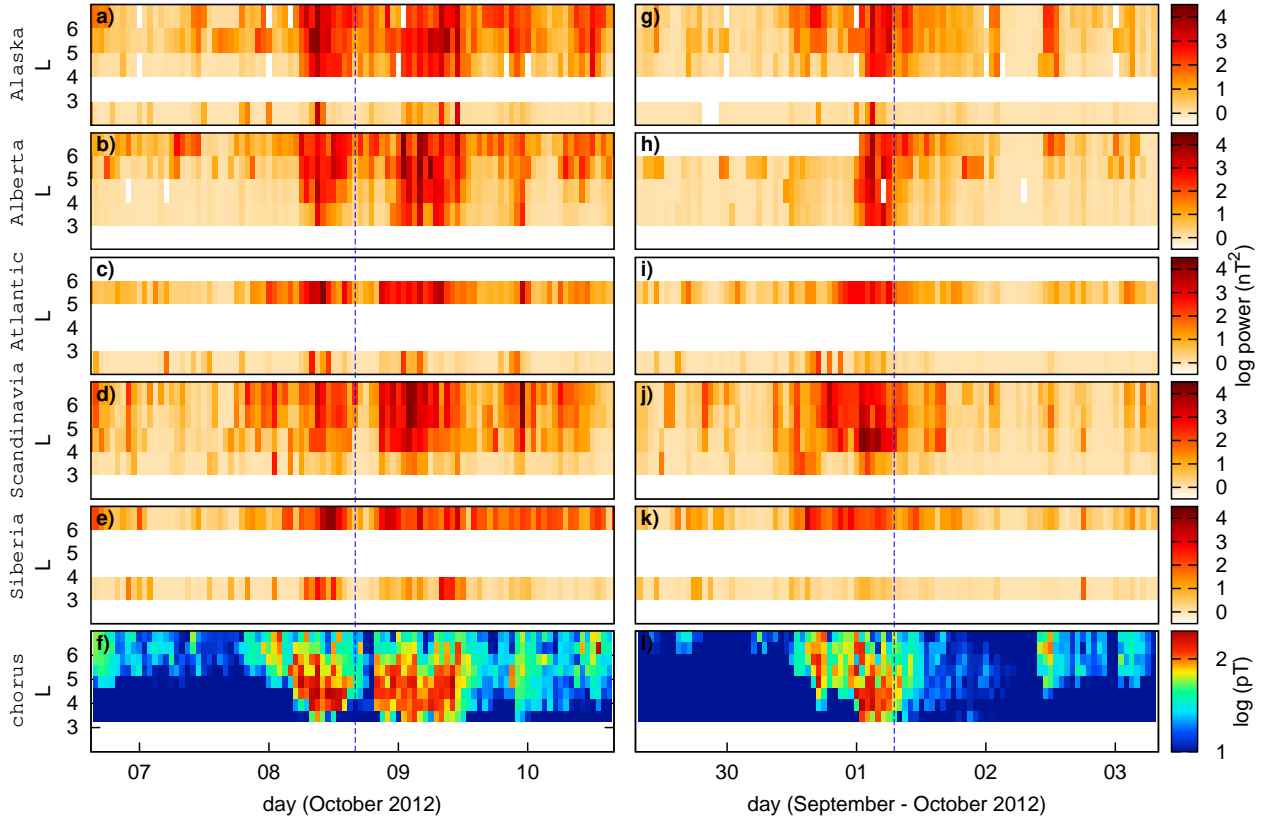


Figure 2. (panels a-e) ULF wave power for a representative efficient acceleration (EA) event during the 8-9 October 2012 storm, each panel showing data as a function of L-shells in five different longitudinal meridians. (panel f) VLF chorus wave amplitude proxy, averaged over all MLT sectors, from L15. The blue line indicates the zero epoch time (see text for details). Panels (g-l) as in panels (a-f) but for a representative inefficient acceleration (IA) event on 1 October 2012.

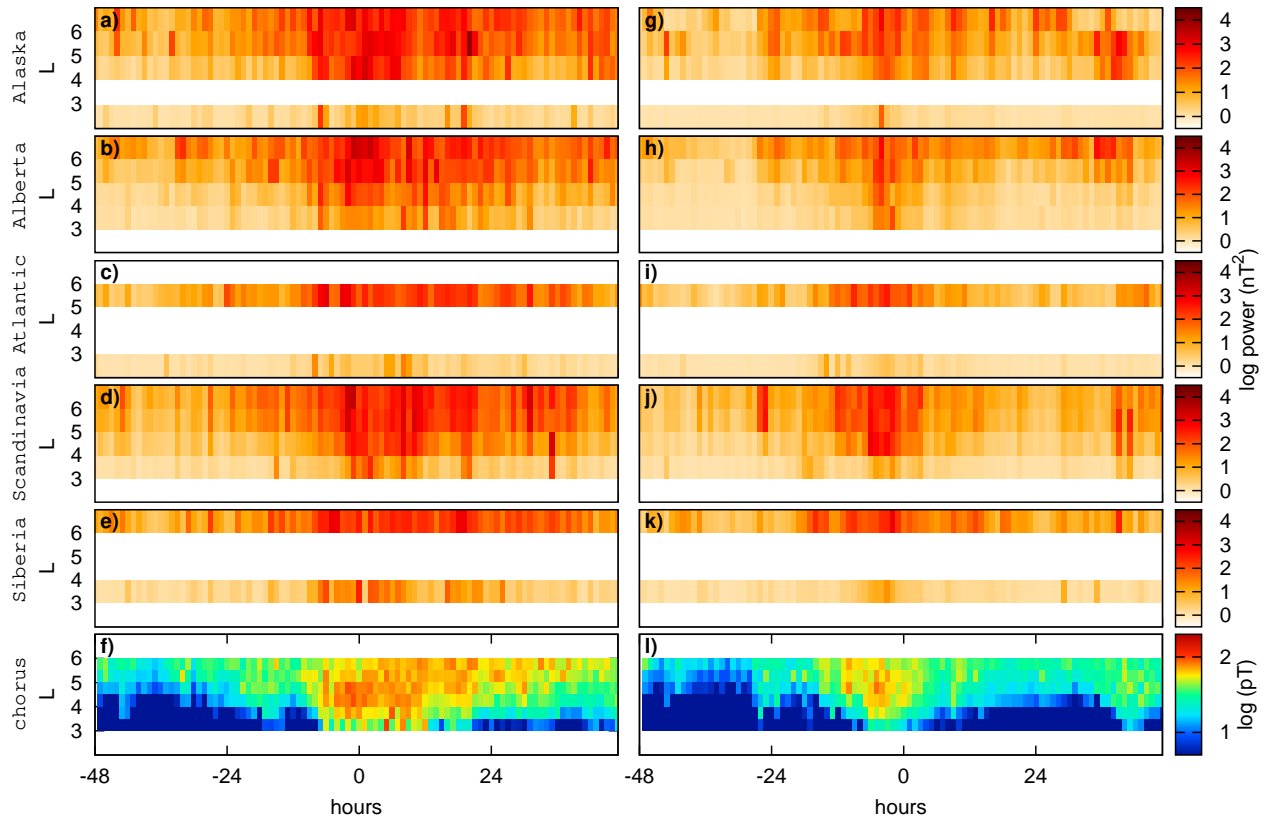


Figure 3. Superposed epoch analysis of ULF wave power as a function L-shell and time in five different longitudinal meridians (top five rows of panels), and the VLF chorus wave proxy from L15 (bottom row of panels), for efficient acceleration (EA, panels a-f) and inefficient acceleration (IA, panels g-l) events.

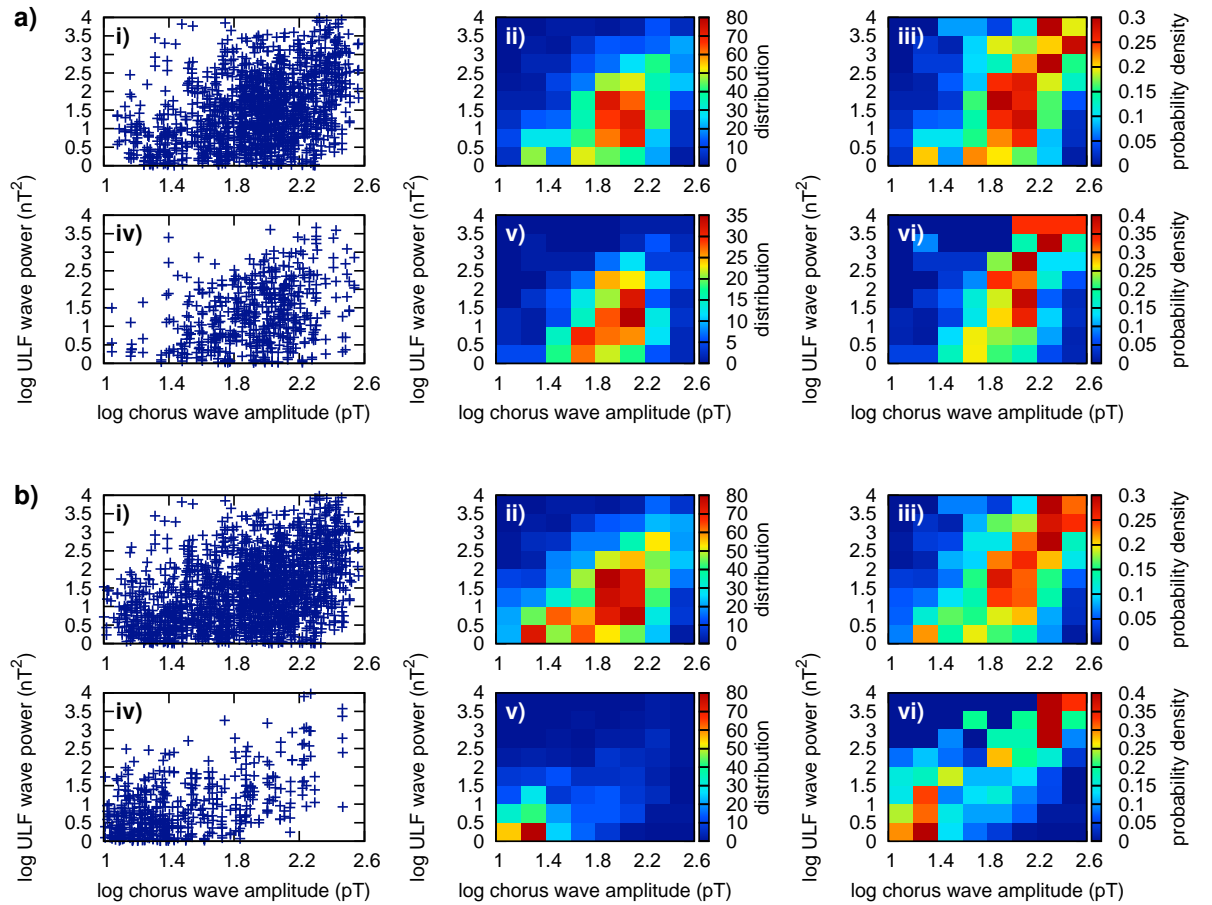


Figure 4. a) L = 5 to 6: i) Scatterplot of integrated Pc5 ULF power measurements compared to the VLF chorus wave amplitude proxy for all EA events; ii) histogram of the scatterplot at (i); iii) probability distribution of VLF chorus wave amplitude proxy as a function of ULF power measurements for all EA events. iv-vi) as in (i-iii) but for all IA events. b) as in (a) but for L = 4 to 5.

As shown in the supplementary material, for the bands $L = 4$ to 5 and $L = 5$ to 6 , Pearson correlation coefficients between ULF and VLF wave proxy values peak at zero temporal offset, with $r = 0.65$ to 0.84 and the p-values for the statistical significance of the null hypothesis ranging from $p = 3 \cdot 10^{-8}$ to $p < 10^{-16}$, using a 2-tailed test of significance. Of course the sample size is large, but this indicates that the connection between the VLF proxy and ULF wave power was very unlikely to have occurred by chance. Figure S36 in the Supplementary material illustrates the meridian dependence, showing the ULF wave global coherence between Albertan and Scandinavian meridian ULF wave power. The fractional variance is consistent in log-log space, and even though some inherent variability exists, likely stemming from MLT dependence, it is dwarfed by the coherent variability of ULF wave power through the course of the storms. Therefore, overall, Figure S36 shows an obvious coherence between ULF waves observed in both meridians.

4 Discussion

A correlation between a VLF wave proxy, derived from POES electron precipitation, and radiation belt electron acceleration events has previously been used by L15 to argue VLF waves play an essential role. Here we show that both the VLF wave proxy and the ULF wave power have common profiles in L-shell and time, not only statistically in relation to their characteristics during radiation belt electron efficient acceleration (EA) and inefficient acceleration (IA) events, but also in each of the 33 individual storms examined by L15. Moreover, the ULF wave power when analysed across multiple meridians tends to show a rather remarkable global coherence as a function of MLT, which suggests that data-driven radial diffusion coefficients might be able to be derived not only historically but also in near-real time using data from stations from a small number of meridians.

Our analysis shows that the question of whether ULF or chorus waves are responsible for electron acceleration is far from settled, and certainly challenges the interpretation of L15 that the VLF waves should be identified as definitively playing a key role in electron acceleration. Of course VLF chorus waves might be important, but given the results presented here they cannot necessarily be identified as the dominant acceleration process based on the characteristics of the VLF proxy during EA and IA events alone.

The strong and clear correlation between ULF wave power and the L15 chorus proxy invites the following possible explanations:

1. chorus waves emerge first and cause a growth of ULF waves;
2. ULF waves emerge first and cause a growth of chorus waves;
3. both ULF and chorus waves are driven with identical L-shell and time profiles by some common solar wind and/or magnetospheric driver which drives both in the same place at the same time;
4. ULF waves can have a direct impact on radiation belt electron precipitation, which pollutes the POES precipitation proxy which is used to infer the presence of VLF chorus waves.

Case 1 is implausible, because chorus waves contain much less energy than ULF waves. Case 2, on the other hand, has some observational and theoretical basis [*Li et al.*, 2011, and references therein]. For example, compressional Pc4-5 pulsations have been found to produce conditions that encourage the production or modulation of chorus waves. If the reservoir of energy in ULF waves can act to locally produce VLF waves, or encourage their more efficient growth, then this would be a natural

explanation for the observations. However, we are not aware of any processes through which ULF waves can directly produce chorus emissions.

Case 3 is less restraining than the previous two cases, since the only correlation needed between the two wave types is temporal, so long as the driving processes act to produce both wave modes in the same place. Chorus waves are assumed to be excited near the Earth's geomagnetic equator by cyclotron resonant interactions with electrons that are anisotropically injected into the plasma sheet during geomagnetically active conditions, either preceding a substorm onset in the dawnside [Lyons *et al.*, 2005; Hwang *et al.*, 2007], or following a substorm onset near midnight [Smith *et al.*, 1999]. ULF waves in the Pc5 frequency range have also been observed to be more prominent in the dawnside [Anderson *et al.*, 1990; Ruohoniemi *et al.*, 1991; Glassmeier and Stellmacher, 2000], generated either by shear flow instabilities along the magnetopause [Cahill and Winckler, 1992; Mann *et al.*, 1999], or more generally in the dayside magnetosphere by variations in solar wind dynamic pressure [Lysak and Lee, 1992]. These studies suggest that the conditions which lead to the excitation of ULF and VLF waves are not necessarily the same, and in our view it is challenging to explain the observed close correspondence of the ULF waves and the VLF wave proxy in terms of a common driver.

Case 4 would require a mechanism with which ULF waves directly cause electron precipitation, thereby being (at least partially) responsible for polluting the chorus wave proxy. One such mechanism has been proposed by Rae *et al.* [2018], whereby localized compressional ULF waves modulate the loss cone, bringing it within reach of a wider range of equatorial pitch angles for energetic particles. Thus, although the correlation between ULF waves and the VLF proxy that we found is mostly global, it is possible that such local effects within more general ULF wave production events may affect precipitation. Indeed, the nature of storm-time ULF waves [e.g., Anderson *et al.*, 1990; Dai *et al.*, 2015] which might be associated with precipitation is an important topic for future study. That is not to say that chorus waves do not exist during some times when precipitation is observed by POES; indeed satellite measurements have, on several occasions, shown chorus waves in correlation with those inferred using the precipitation VLF proxy [Li *et al.*, 2013, 2016]. Rather, the precise level of VLF wave power and the spatial and temporal configuration of the inferred VLF waves may be modified by the effects of ULF wave-driven precipitation on the proxy. A further complicating factor is the degradation of the POES MEPED proton detectors [e.g., Galand and Evans, 2000; Ødegaard *et al.*, 2016], whose directional dependence may affect the L15 VLF proxy.

Overall, our results show a rather remarkable correspondence between the VLF chorus wave proxy [Li *et al.*, 2013], as applied in L15, and the distributions of global ULF wave power in all 33 storms where such a comparison was feasible. We note similar results by Katsavrias *et al.* [2015], who examined only a single EA and IA event, and that of Ma *et al.* [2018] but without a discussion on morphological similarities. This not only reveals further challenges with identifying the dominant and causative agents of radiation belt electron acceleration during storm time events, but also suggests the possibility of a much closer relationship between VLF waves and ULF waves in the inner magnetosphere than has previously been thought. Of course, it is possible that the reported correspondence between the VLF wave proxy and the observed ULF wave power is explained as a result of direct ULF wave driven precipitation polluting the VLF wave proxy. More work is needed to examine these inter-relationships further, but certainly our results suggest that care should be taken when using the POES precipitation measurements as a mechanism to derive a proxy for VLF wave amplitudes in the inner magnetosphere.

Acknowledgments

SD was supported by the Canadian Space Agency Geospace Observatory (GO) Canada program. IRM is supported by a Discovery Grant from Canadian NSERC. We thank Dr Wen Li for processed POES Chorus wave proxy data, as well as for her useful comments on the manuscript. The data in this letter are available at https://osf.io/xdpf8/?view_only=b0d7daa8b0ba488fae493d9ec1a729e4. All magnetometer data used are available from SuperMAG at <http://supermag.jhuapl.edu/mag>. For the magnetometer data we gratefully thank: USGS, Jeffrey J. Love; CARISMA, PI Ian Mann; AARI, PI Oleg Troshichev; GIMA; The institutes who maintain the IMAGE magnetometer array, PI Eija Tanskanen; AUTUMN, PI Martin Connors; DTU Space, PI Dr. Rico Behlke; CANMOS; THEMIS, PI Vassilis Angelopoulos.

References

- Anderson, B. J., M. J. Engebretson, S. P. Rounds, L. J. Zanetti, and T. A. Potemra (1990), A statistical study of Pc 3-5 pulsations observed by the AMPTE/CCE magnetic fields experiment. I - Occurrence distributions, *Journal of Geophysical Research*, *95*, 10,495–10,523, doi:10.1029/JA095iA07p10495.
- Baker, D. N. (1998), What is space weather?, *Advances in Space Research*, *22*, 7–16, doi:10.1016/S0273-1177(97)01095-8.
- Baker, D. N., S. G. Kanekal, V. C. Hoxie, S. Batiste, M. Bolton, X. Li, S. R. Elkington, S. Monk, R. Reukauf, S. Steg, J. Westfall, C. Belting, B. Bolton, D. Braun, B. Cervelli, K. Hubbell, M. Kien, S. Knappmiller, S. Wade, B. Lamprecht, K. Stevens, J. Wallace, A. Yehle, H. E. Spence, and R. Friedel (2013), The Relativistic Electron-Proton Telescope (REPT) Instrument on Board the Radiation Belt Storm Probes (RBSP) Spacecraft: Characterization of Earth's Radiation Belt High-Energy Particle Populations, *Space Science Reviews*, *179*, 337–381, doi:10.1007/s11214-012-9950-9.
- Brautigam, D. H., and J. M. Albert (2000), Radial diffusion analysis of outer radiation belt electrons during the October 9, 1990, magnetic storm, *Journal of Geophysical Research*, *105*, 291–310, doi:10.1029/1999JA900344.
- Cahill, L. J., Jr., and J. R. Winckler (1992), Periodic magnetopause oscillations observed with the GOES satellites on March 24, 1991, *Journal of Geophysical Research*, *97*, 8239–8243, doi:10.1029/92JA00433.
- Choi, H.-S., J. Lee, K.-S. Cho, Y.-S. Kwak, I.-H. Cho, Y.-D. Park, Y.-H. Kim, D. N. Baker, G. D. Reeves, and D.-K. Lee (2011), Analysis of GEO spacecraft anomalies: Space weather relationships, *Space Weather*, *9*, 06001, doi:10.1029/2010SW000597.
- Cunningham, G. S. (2016), Radial diffusion of radiation belt particles in nondipolar magnetic fields, *Journal of Geophysical Research (Space Physics)*, *121*, 5149–5171, doi:10.1002/2015JA021981.
- Daglis, I., D. Baker, J. Kappenman, M. Panasyuk, and E. Daly (2004), Effects of space weather on technology infrastructure, *Space Weather*, *2*, S02004, doi:10.1029/2003SW000044.
- Dai, L., K. Takahashi, R. Lysak, C. Wang, J. R. Wygant, C. Kletzing, J. Bonnell, C. A. Cattell, C. W. Smith, R. J. MacDowall, S. Thaller, A. Breneman, X. Tang, X. Tao, and L. Chen (2015), Storm time occurrence and spatial distribution of Pc4 poloidal ULF waves in the inner magnetosphere: A Van Allen Probes statistical study, *Journal of Geophysical Research (Space Physics)*, *120*, 4748–4762, doi:10.1002/2015JA021134.
- Elkington, S. R., M. K. Hudson, and A. A. Chan (1999), Acceleration of relativistic electrons via drift-resonant interaction with toroidal-mode Pc-5 ULF oscillations, *Geophysical Research Letters*, *26*, 3273–3276, doi:10.1029/1999GL003659.
- Fälthammar, C.-G. (1965), Effects of Time-Dependent Electric Fields on Geomagnetically Trapped Radiation, *Journal of Geophysical Research*, *70*, 2503–2516, doi:

- 10.1029/JZ070i011p02503.
- Fei, Y., A. A. Chan, S. R. Elkington, and M. J. Wiltberger (2006), Radial diffusion and MHD particle simulations of relativistic electron transport by ULF waves in the September 1998 storm, *Journal of Geophysical Research (Space Physics)*, *111*, A12209, doi:10.1029/2005JA011211.
- Galand, M., and D. Evans (2000), Radiation damage of the proton meped detector on poes (tiros/noaa) satellites, *NOAA Technical Report OAR*.
- Gjerloev, J. W. (2009), A Global Ground-Based Magnetometer Initiative, *EOS Transactions*, *90*, 230–231, doi:10.1029/2009EO270002.
- Gjerloev, J. W. (2012), The SuperMAG data processing technique, *Journal of Geophysical Research (Space Physics)*, *117*, A09213, doi:10.1029/2012JA017683.
- Glassmeier, K.-H., and M. Stellmacher (2000), Concerning the local time asymmetry of Pc5 wave power at the ground and field line resonance widths, *Journal of Geophysical Research*, *105*, 18, doi:10.1029/2000JA900037.
- Horne, R. B., and R. M. Thorne (1998), Potential waves for relativistic electron scattering and stochastic acceleration during magnetic storms, *Geophysical Research Letters*, *25*, 3011–3014, doi:10.1029/98GL01002.
- Horne, R. B., R. M. Thorne, Y. Y. Shprits, N. P. Meredith, S. A. Glauert, A. J. Smith, S. G. Kanekal, D. N. Baker, M. J. Engebretson, J. L. Posch, M. Spasojevic, U. S. Inan, J. S. Pickett, and P. M. E. Decreau (2005), Wave acceleration of electrons in the Van Allen radiation belts, *Nature*, *437*, 227–230, doi:10.1038/nature03939.
- Huang, C.-L., H. E. Spence, M. K. Hudson, and S. R. Elkington (2010), Modeling radiation belt radial diffusion in ULF wave fields: 2. Estimating rates of radial diffusion using combined MHD and particle codes, *Journal of Geophysical Research (Space Physics)*, *115*, A06216, doi:10.1029/2009JA014918.
- Hudson, M. K., S. R. Elkington, J. G. Lyon, C. C. Goodrich, and T. J. Rosenberg (1999), Simulation of radiation belt dynamics driven by solar wind variations, *Washington DC American Geophysical Union Geophysical Monograph Series*, *109*, 171–182, doi:10.1029/GM109p0171.
- Hwang, J. A., D.-Y. Lee, L. R. Lyons, A. J. Smith, S. Zou, K. W. Min, K.-H. Kim, Y.-J. Moon, and Y. D. Park (2007), Statistical significance of association between whistler-mode chorus enhancements and enhanced convection periods during high-speed streams, *Journal of Geophysical Research (Space Physics)*, *112*, A09213, doi:10.1029/2007JA012388.
- Katsavrias, C., I. A. Daglis, W. Li, S. Dimitrakoudis, M. Georgiou, D. L. Turner, and C. Papadimitriou (2015), Combined effects of concurrent Pc5 and chorus waves on relativistic electron dynamics, *Annales Geophysicae*, *33*, 1173–1181, doi:10.5194/angeo-33-1173-2015.
- Li, W., R. M. Thorne, J. Bortnik, Y. Nishimura, and V. Angelopoulos (2011), Modulation of whistler mode chorus waves: 1. Role of compressional Pc4-5 pulsations, *Journal of Geophysical Research (Space Physics)*, *116*, A06205, doi:10.1029/2010JA016312.
- Li, W., B. Ni, R. M. Thorne, J. Bortnik, J. C. Green, C. A. Kletzing, W. S. Kurth, and G. B. Hospodarsky (2013), Constructing the global distribution of chorus wave intensity using measurements of electrons by the POES satellites and waves by the Van Allen Probes, *Geophysical Research Letters*, *40*, 4526–4532, doi:10.1002/grl.50920.
- Li, W., R. M. Thorne, Q. Ma, B. Ni, J. Bortnik, D. N. Baker, H. E. Spence, G. D. Reeves, S. G. Kanekal, J. C. Green, C. A. Kletzing, W. S. Kurth, G. B. Hospodarsky, J. B. Blake, J. F. Fennell, and S. G. Claudepierre (2014), Radiation belt electron acceleration by chorus waves during the 17 March 2013 storm, *Journal of Geophysical Research (Space Physics)*, *119*, 4681–4693, doi:10.1002/2014JA019945.
- Li, W., R. M. Thorne, J. Bortnik, D. N. Baker, G. D. Reeves, S. G. Kanekal, H. E. Spence, and J. C. Green (2015), Solar wind conditions leading to efficient radia-

- tion belt electron acceleration: A superposed epoch analysis, *Geophysical Research Letters*, *42*, 6906–6915, doi:10.1002/2015GL065342.
- Li, W., Q. Ma, R. M. Thorne, J. Bortnik, X.-J. Zhang, J. Li, D. N. Baker, G. D. Reeves, H. E. Spence, C. A. Kletzing, W. S. Kurth, G. B. Hospodarsky, J. B. Blake, J. F. Fennell, S. G. Kanekal, V. Angelopoulos, J. C. Green, and J. Goldstein (2016), Radiation belt electron acceleration during the 17 March 2015 geomagnetic storm: Observations and simulations, *Journal of Geophysical Research (Space Physics)*, *121*, 5520–5536, doi:10.1002/2016JA022400.
- Lyons, L. R., D.-Y. Lee, R. M. Thorne, R. B. Horne, and A. J. Smith (2005), Solar wind-magnetosphere coupling leading to relativistic electron energization during high-speed streams, *Journal of Geophysical Research (Space Physics)*, *110*, A11202, doi:10.1029/2005JA011254.
- Lysak, R. L., and D.-H. Lee (1992), Response of the dipole magnetosphere to pressure pulses, *Geophysical Research Letters*, *19*, 937–940, doi:10.1029/92GL00625.
- Ma, Q., W. Li, J. Bortnik, R. M. Thorne, X. Chu, L. G. Ozeke, G. D. Reeves, C. A. Kletzing, W. S. Kurth, G. B. Hospodarsky, M. J. Engebretson, H. E. Spence, D. N. Baker, J. B. Blake, J. F. Fennell, and S. G. Claudepierre (2018), Quantitative evaluation of radial diffusion and local acceleration processes during geom challenge events, *Journal of Geophysical Research: Space Physics*, *0(0)*, doi:10.1002/2017JA025114.
- Mann, I. R., A. N. Wright, K. J. Mills, and V. M. Nakariakov (1999), Excitation of magnetospheric waveguide modes by magnetosheath flows, *Journal of Geophysical Research*, *104*, 333–354, doi:10.1029/1998JA900026.
- Mann, I. R., L. G. Ozeke, K. R. Murphy, S. G. Claudepierre, D. L. Turner, D. N. Baker, I. J. Rae, A. Kale, D. K. Milling, A. J. Boyd, H. E. Spence, G. D. Reeves, H. J. Singer, S. Dimitrakoudis, I. A. Daglis, and F. Honary (2016), Explaining the dynamics of the ultra-relativistic third Van Allen radiation belt, *Nature Physics*, *12*, 978–983, doi:10.1038/nphys3799.
- Mathie, R. A., and I. R. Mann (2000), A correlation between extended intervals of ULF wave power and storm-time geosynchronous relativistic electron flux enhancements, *Geophysical Research Letters*, *27*, 3261–3264, doi:10.1029/2000GL003822.
- Murphy, K. R., I. R. Mann, I. J. Rae, D. G. Sibeck, and C. E. J. Watt (2016), Accurately characterizing the importance of wave-particle interactions in radiation belt dynamics: The pitfalls of statistical wave representations, *Journal of Geophysical Research (Space Physics)*, *121*, 7895–7899, doi:10.1002/2016JA022618.
- Ni, B., W. Li, R. M. Thorne, J. Bortnik, J. C. Green, C. A. Kletzing, W. S. Kurth, G. B. Hospodarsky, and M. Soria-Santacruz Pich (2014), A novel technique to construct the global distribution of whistler mode chorus wave intensity using low-altitude POES electron data, *Journal of Geophysical Research (Space Physics)*, *119*, 5685–5699, doi:10.1002/2014JA019935.
- Ødegaard, L.-K. G., H. N. Tyssøy, M. I. Jakobsen Sandanger, J. Stadsnes, and F. Søråas (2016), Space Weather impact on the degradation of NOAA POES MEPED proton detectors, *Journal of Space Weather and Space Climate*, *6(27)*, A26, doi:10.1051/swsc/2016020.
- Ozeke, L. G., I. R. Mann, K. R. Murphy, I. Jonathan Rae, and D. K. Milling (2014), Analytic expressions for ULF wave radiation belt radial diffusion coefficients, *Journal of Geophysical Research (Space Physics)*, *119*, 1587–1605, doi:10.1002/2013JA019204.
- Perry, K. L., M. K. Hudson, and S. R. Elkington (2005), Incorporating spectral characteristics of Pc5 waves into three-dimensional radiation belt modeling and the diffusion of relativistic electrons, *Journal of Geophysical Research (Space Physics)*, *110*, A03215, doi:10.1029/2004JA010760.
- Rae, I. J., I. R. Mann, K. R. Murphy, L. G. Ozeke, D. K. Milling, A. A. Chan, S. R. Elkington, and F. Honary (2012), Ground-based magnetometer determination of in situ Pc4-5 ULF electric field wave spectra as a function of solar wind speed, *Journal*

- of *Geophysical Research (Space Physics)*, 117, A04221, doi:10.1029/2011JA017335.
- Rae, I. J., K. R. Murphy, C. E. J. Watt, A. J. Halford, I. R. Mann, L. G. Ozeke, D. G. Sibeck, M. A. Clilverd, C. J. Rodger, A. W. Degeling, C. Forsyth, and H. J. Singer (2018), The Role of Localized Compressional Ultra-low Frequency Waves in Energetic Electron Precipitation, *Journal of Geophysical Research (Space Physics)*, 123, 1900–1914, doi:10.1002/2017JA024674.
- Reeves, G. D., H. E. Spence, M. G. Henderson, S. K. Morley, R. H. W. Friedel, H. O. Funsten, D. N. Baker, S. G. Kanekal, J. B. Blake, J. F. Fennell, S. G. Claudepierre, R. M. Thorne, D. L. Turner, C. A. Kletzing, W. S. Kurth, B. A. Larsen, and J. T. Niehof (2013), Electron Acceleration in the Heart of the Van Allen Radiation Belts, *Science*, 341, 991–994, doi:10.1126/science.1237743.
- Ruohoniemi, J. M., R. A. Greenwald, K. B. Baker, and J. C. Samson (1991), HF radar observations of Pc 5 field line resonances in the midnight/early morning MLT sector, *Journal of Geophysical Research*, 96, 15, doi:10.1029/91JA00795.
- Sarno-Smith, L. K., B. A. Larsen, R. M. Skoug, M. W. Liemohn, A. Breneman, J. R. Wygant, and M. F. Thomsen (2016), Spacecraft surface charging within geosynchronous orbit observed by the Van Allen Probes, *Space Weather*, 14, 151–164, doi:10.1002/2015SW001345.
- Schulz, M., and L. J. Lanzerotti (1974), Particle Diffusion in the Radiation Belts, *Physics and Chemistry in Space*, 7, doi:10.1007/978-3-642-65675-0.
- Smith, A. J., M. P. Freeman, M. G. Wickett, and B. D. Cox (1999), On the relationship between the magnetic and VLF signatures of the substorm expansion phase, *Journal of Geophysical Research*, 104, 12,351–12,360, doi:10.1029/1998JA900184.
- Spence, H. E., G. D. Reeves, D. N. Baker, J. B. Blake, M. Bolton, S. Bourdarie, A. A. Chan, S. G. Claudepierre, J. H. Clemmons, J. P. Cravens, S. R. Elkington, J. F. Fennell, R. H. W. Friedel, H. O. Funsten, J. Goldstein, J. C. Green, A. Guthrie, M. G. Henderson, R. B. Horne, M. K. Hudson, J.-M. Jahn, V. K. Jordanova, S. G. Kanekal, B. W. Klatt, B. A. Larsen, X. Li, E. A. MacDonald, I. R. Mann, J. Niehof, T. P. O'Brien, T. G. Onsager, D. Salvaggio, R. M. Skoug, S. S. Smith, L. L. Suther, M. F. Thomsen, and R. M. Thorne (2013), Science Goals and Overview of the Radiation Belt Storm Probes (RBSP) Energetic Particle, Composition, and Thermal Plasma (ECT) Suite on NASA's Van Allen Probes Mission, *Space Science Reviews*, 179, 311–336, doi:10.1007/s11214-013-0007-5.
- Summers, D., C. Ma, N. P. Meredith, R. B. Horne, R. M. Thorne, D. Heynderickx, and R. R. Anderson (2002), Model of the energization of outer-zone electrons by whistler-mode chorus during the October 9, 1990 geomagnetic storm, *Geophysical Research Letters*, 29, 2174, doi:10.1029/2002GL016039.
- Tao, X., J. M. Albert, and A. A. Chan (2009), Numerical modeling of multidimensional diffusion in the radiation belts using layer methods, *Journal of Geophysical Research (Space Physics)*, 114, A02215, doi:10.1029/2008JA013826.
- Thorne, R. M., W. Li, B. Ni, Q. Ma, J. Bortnik, L. Chen, D. N. Baker, H. E. Spence, G. D. Reeves, M. G. Henderson, C. A. Kletzing, W. S. Kurth, G. B. Hospodarsky, J. B. Blake, J. F. Fennell, S. G. Claudepierre, and S. G. Kanekal (2013), Rapid local acceleration of relativistic radiation-belt electrons by magnetospheric chorus, *Nature*, 504, 411–414, doi:10.1038/nature12889.
- Tu, W., G. S. Cunningham, Y. Chen, S. K. Morley, G. D. Reeves, J. B. Blake, D. N. Baker, and H. Spence (2014), Event-specific chorus wave and electron seed population models in DREAM3D using the Van Allen Probes, *Geophysical Research Letters*, 41, 1359–1366, doi:10.1002/2013GL058819.
- Turner, D. L., Y. Shprits, M. Hartinger, and V. Angelopoulos (2012), Explaining sudden losses of outer radiation belt electrons during geomagnetic storms, *Nature Physics*, 8, 208–212, doi:10.1038/nphys2185.
- Ukhorskiy, A. Y., M. I. Sitnov, K. Takahashi, and B. J. Anderson (2009), Radial transport of radiation belt electrons due to stormtime Pc5 waves, *Annales Geophysicae*,

27, 2173–2181, doi:10.5194/angeo-27-2173-2009.
Webb, D., and J. Allen (2004), Spacecraft and Ground Anomalies Related to the
October–November 2003 Solar Activity, *Space Weather*, 2, S03008, doi:10.1029/
2004SW000075.